Hydration thermodynamics of pyrochlore structured oxides from TG and first principles calculations

Tor S. Bjørheim, Vasileios Besikiotis and Reidar Haugsrud[*]

Department of Chemistry, University of Oslo, FERMiO, Gaustadallèen 21, NO-0349 Oslo, Norway

Abstract

In this work we discuss trends in the defect chemistry and hydration thermodynamics of rare-earth pyrochlore structured oxides, $RE_2X_2O_7$ (RE = La-Lu and X = Ce, Zr, Sn, Ti). Density Functional Theory (DFT) calculations have been performed to elucidate trends in the general defect chemistry and hydration enthalpy for the abovementioned series. Further, to justify the use of such theoretical methods, the hydration properties of selected compositions were studied by means of thermogravimetric measurements. Both from DFT calculations and TG measurements, the hydration enthalpy becomes less exothermic with decreasing radii of RE-ions within the $RE_2X_2O_7$ series (X=Ti, Sn, Zr, Ce). However, changing the X-site ion has smaller effect on the hydration enthalpies. The observed hydration trends are discussed in connection with trends in the stability of both protons and oxygen vacancies and changes in the electronic density of states and bonding environment through the series. Finally, the findings are discussed with respect to existing correlations for other binary and ternary rare-earth oxides.

Keywords: Pyrochlore, TG, DFT, defects, protons, hydration

**Corresponding author: reidarha@kjemi.uio.no*

1 Introduction

Oxide ceramics display numerous functional properties which are widely utilized in applications covering a range of fields from low temperature photocatalytic applications to high temperature solid oxide fuel cells. Hydrogen, being omnipresent as either H_2(g) or H_2O(g), is often found as a dominating defect in form of protonic defects ($OH_O^{\bullet}$) in various oxides. Hydration of oxygen vacancies ($v_O^{\bullet\bullet}$) is the most commonly parameterized equilibrium for incorporation of these protonic defects;

$$H_2O(g) + v_O^{\bullet\bullet} + O_O^{\times} = 2OH_O^{\bullet} \quad (1)$$

with an equilibrium constant given by;

$$K_{\mathrm{Hydr}} = \frac{a_{OH_O^{\bullet}}^2}{a_{v_O^{\bullet\bullet}} a_{O_O^{\times}} a_{H_2O}} = \exp\left(-\frac{\Delta_{\mathrm{hydr}}G^0}{RT}\right) = \exp\left(\frac{\Delta_{\mathrm{hydr}}S^0}{R}\right)\exp\left(-\frac{\Delta_{\mathrm{hydr}}H^0}{RT}\right) \quad (2)$$

where a_i is the activity of each species, and $\Delta_{\mathrm{hydr}}S^0$ and $\Delta_{\mathrm{hydr}}H^0$ are the standard hydration entropy and enthalpy, respectively. While the hydration entropy typically is reported to attain values of -120±40 J/molK [1], the hydration enthalpy ranges from -220 kJ/mol for Y_2O_3 and Er_2O_3[2] which hydrate to temperatures above 1000 °C, to moderately exothermic and even positive values in ZrO_2 or CeO_2[1]. Over the last decades it has been shown that many ceramic oxides display significant proton conduction, even at temperatures up to 1000 °C. The most commonly studied oxides are those crystallizing in the perovskite structure (ABO_3) where systems such as acceptor doped $BaZrO_3$, $BaCeO_3$ and $SrCeO_3$ display proton conductivities in the order of 10^{-2} S/cm at 800 °C[3-5]. However, the applicability of these oxides is limited by high grain boundary resistance and instability towards CO_2, and at moderate temperatures also towards H_2O. Although various non-Ba containing oxides, for instance within the monazite ($LaPO_4$[6], $LaVO_4$[7] and $LaAsO_4$[8]) and scheelite ($LaNbO_4$) families[9, 10], and in the rare-earth pyrochlore family of oxides, $RE_2X_2O_7$ (X=Ti, Sn, Zr)[11-14], display proton conduction, the partial proton conductivity these generally peaks at lower values than those of the state-of-the-art perovskites**.** Acceptor doped $La_2Zr_2O_7$ is the most widely studied rare-earth based pyrochlore oxide in terms of proton conduction [11, 15-17] and displays, e.g. a maximum proton conductivity of $5{\cdot}10^{-4}$ S/cm.

In the search for materials with high proton conductivity, a more fundamental understanding of possible correlations between hydration and proton transport in the oxides and other fundamental properties such as elemental composition and structure has been sought during

Field Code Changed
Field Code Changed
Field Code Changed
Field Code Changed
Field Code Changed
Field Code Changed
Field Code Changed
Field Code Changed
Field Code Changed
Field Code Changed
Field Code Changed

the two last decades. The hydration equilibrium may be viewed as a two-step process in which an oxide ion vacancy first is filled by an oxide ion, followed by protonation of two lattice oxide ions;

$$v_O^{\bullet\bullet} + 2e^{/} + \tfrac{1}{2}O_2(g) = O_O^{\times} \quad (3)$$

$$H_2O(g) + 2O_O^{\times} = 2OH_O^{\bullet} + 2e^{/} + \tfrac{1}{2}O_2(g) \quad (4)$$

Both processes may be regarded as Lewis acid/base reactions, and an oxide's hydration properties are often linked to its basicity through the electronegativity of the cations (for instance in case of perovskites [4]). However, in other series such as rare-earth sesquioxides and niobates, it is to a large extent the size of the cations which determines the hydration properties [2, 18]. These two rather different empirical correlations reflect the intricate nature of the hydration thermodynamics of oxides, which we will elaborate on in the following literature section.

Field Code Changed
Field Code Changed
Field Code Changed

2 Hydration trends of binary and ternary oxides

For the perovskite series $Ba(Ce_{x-1}Y_x)O_{3-d}$ and $Ba_2(Sn_{1-x}Y_x)_2O_{3-d}$, Kreuer[4] reported an increasingly exothermic hydration enthalpy with increasing Y content, which was attributed to increasing basicity of the oxide ions. This observation has later been supported by computational charge density analyses on Y doped $BaCeO_3$[19] showing increasing charge of the oxygen ions with increasing Y content. Norby *et al.*[1] proposed a more general correlation relating hydration of oxygen vacancies to the difference between the electronegativity of the B and A site cations within the perovskite series; The smaller the difference, the more exothermic the hydration enthalpy is. It has later been argued that the correlation also holds for both systems in which B is more electronegative than A, and vice versa [20]. The hydration enthalpy has also been correlated with the Goldschmidt's tolerance factor of the perovskites; the lower the tolerance factor, the more exothermic the hydration enthalpy [20].

Field Code Changed
Field Code Changed
Field Code Changed
Field Code Changed
Field Code Changed

In case of the rare-earth sesquioxides, RE_2O_3, Norby and Larring[2, 21] showed that the enthalpy of hydration according to Eq. 1 becomes more exothermic with decreasing size of the RE-ion (and thus decreasing stability of the oxides), attributed to decreasing stability of oxygen vacancies.

Field Code Changed
Field Code Changed

For the scheelite structured rare-earth ortho-niobates, $RENbO_4$, Haugsrud and Norby[18] also showed that the hydration enthalpies become more exothermic with decreasing size of the RE

Field Code Changed

ion. Further, for the structurally similar monazites, $LaXO_4$ (X=P, As, V), only minor dependence of the hydration enthalpy on the X-site element was encountered[7, 8], thus showing that the two cations do not affect the hydration enthalpy in a 'simple' manner, such as for the perovskites.

For pyrochlore structured oxides, trends in the hydration thermodynamics are more unclear, and it is important to recognize that the structure may change within the series of materials. Knee *et al.*[13] investigated the $Sm_2X_2O_7$ series (X=Ti, Sn, Zr and Ce) and found that the hydration thermodynamics were dependent on the X-site element, with the smaller cations displaying the highest levels of hydration. Furthermore for the RE-site, $Sm_2Ti_2O_7$[13] exhibits higher proton conductivity than $Er_2Ti_2O_7$ which only displays a minor contribution from protons to the bulk conductivity at the lowest temperatures (t<350°C)[22]. This suggests that the hydration enthalpy increases (less negative) with decreasing size of the RE ion, *i.e.* opposite to the rare-earth niobates. In this respect, it is interesting to note that the trends in formation enthalpy for the two series of compounds still concur; the formation enthalpy increases (less stable oxides) with decreasing RE size. Within the pyrochlore series, the deviation from the ideal pyrochlore structure has been related to the the r_{RE}/r_X ratio, and the degree of anion and cation disorder increases when the ratio decreases[23, 24]. In this respect, Besikiotis *et al.*[25] recently showed that the hydration enthalpies of the two end-members in the series $La_2(Ce_xZr_{1-x})_2O_7$ (x=0 and x=1) were similar, whereas that of the substituted compositions were less exothermic. The behavior was attributed to the gradual ordering of the cation and anion lattice with increasing Zr content.

As trends in the hydration enthalpy most likely are dependent on structural changes through a series oxides, we have in this work focused on pyrochlore structured oxides which attain the cubic Fd-3m structure for a large variety of compositions. We investigate the general defect chemistry and trends in the hydration thermodynamics through the $RE_2X_2O_7$ (RE=La-Lu, X=Ti, Sn, Zr, Ce) series in detail by first principles density functional theory (DFT) calculations. The observed trends are, moreover, supplemented with thermogravimetric measurements (TG) of the water uptake in selected $RE_2Sn_2O_7$ compositions. The trends are discussed in relation to the bonding environment of protons and oxygen vacancies, charge density of the oxide ions, and changes in the electronic structure upon defect formation. Finally, the characteristics of these pyrochlores are discussed and compared to existing empirical trends for other series of oxides.

Field Code Changed
Field Code Changed
Field Code Changed
Field Code Changed
Field Code Changed
Field Code Changed
Field Code Changed
Field Code Changed

3 Experimental

$La_{1.8}Ca_{0.2}Sn_2O_{7-\delta}$, $Sm_{1.8}Ca_{0.2}Sn_2O_{7-\delta}$ and $Er_{1.8}Ca_{0.2}Sn_2O_{7-\delta}$ were prepared by solid state reaction with La_2O_3 (99.9%), Sm_2O_3 (99.9%), Er_2O_3 (99.9%) supplied by Alfa Aesar. All starting powders were dried at 950 °C for 1 h prior to weighing due to their hygroscopic nature. Stoichiometric amounts of the precursors were ball milled in isopropanol, calcined at 1000 °C for 10 h in air, and finally remixed in a mortar before second calcination at 1350 °C for 10 h. Structural characterization of the as prepared powders was performed by X-Ray Diffraction (XRD), utilizing a Siemens D5000 diffractometer with $CuK_{\alpha 1}$ radiation. All the X-rays patterns could be refined in the pyrochlore (Fd-3m) structure, but also with minor amounts of $CaSnO_3$ indicating that the solubility of Ca in the series of $RE_2Sn_2O_7$ is rather limited.

The relative weight change as function of temperature in wet air (p_{H_2O} = 0.025 atm) was studied by means of thermogravimetry (TG) using a Netzsch STA 449 F1 Jupiter. The measurements were performed isobarically as function of temperature in the range from 1000 to 300 °C. The samples were allowed to equilibrate for 5 h at each temperature, with a cooling rate of 50 °C/h between the temperature steps.

4 Computational methodology

4.1 Computational details

The calculations in this work were performed within the Density Functional Theory (DFT) formalism, using the VASP code[26, 27]. Exchange and correlation effects were described by the Generalized Gradient Approximation functional due to Perdew, Burke and Ernzerhof (GGA-PBE)[28] and the projector augmented-wave (PAW) method for the electron-ion interactions[29]. A constant cut-off energy of 500 eV for the plane-waves was used in all calculations.

Field Code Changed
Field Code Changed
Field Code Changed
Field Code Changed

As the Fd-3m unit cell of $RE_2X_2O_7$ encompasses 88 atoms with lattice constants of 10-11 Å, a single unit cell was used in all calculations. The pristine structures were optimized prior to the defect calculations by relaxing all lattice volumes, shapes and ionic positions until the residual forces were smaller than 0.02 eV/Å, with an energy convergence criterion of 10^{-6} eV for self-consistency.

Phonon calculations of the $OH_O^{\bullet}$ defect and bulk O atoms were performed using accurately optimized structures, for which the convergence criteria were decreased to 10^{-4} eV/Å and 10^{-8}

eV. The vibrational modes were calculated within the harmonic approximation from finite displacements by, in the case of $OH_O^{\bullet}$, allowing full relaxation of the H and the 10 nearest atoms, and for bulk O, displacement of only the O atom itself. A finite displacement length of 0.015 Å in all directions was used for all calculations.

Defect calculations were performed with a single defect in each cell with the total charge adjusted to reflect the desired charge state of the defect. To avoid divergence of the coulomb energy of the overall system, the additional charge was compensated by introduction of a compensating jellium background charge in the supercells. Finally, Bader charge density analyses were performed on selected compositions according to ref. [30].

Field Code Changed

Rare-earth pyrochlores encompass 8 fold coordinated RE and 6 fold coordinated X site cations, two coordination-wise non-equivalent occupied oxygen sites, O48f and O8b, and an unoccupied interstitial site, v_{i8a}. The O48f sites are located in the XO_6 octahedron, and are thus coordinated to both the RE and X site cation, while the O8b sites only are coordinated to the RE cations. Similarly, the unoccupied v_{i8a} sites are coordinated only to the X site cation. Hence, we have in this work considered defect formation at all oxygen sites, *i.e.* v_{O8b}, v_{O48f}, OH_{O8b}, OH_{O48f}, $O_{i8a}^{//}$ and $OH_{i8a}^{/}$.

4.2 Thermodynamic formalism

All defect formation energies were obtained through:

$$\Delta G_{\mathrm{Defect}}^{\mathrm{f}} = E_{\mathrm{Defect}}^{\mathrm{tot}} - E_{\mathrm{Bulk}}^{\mathrm{tot}} \pm \sum_{i=1}^{\mathrm{N}} n_i \mu_{\mathrm{i}} + q(\varepsilon_{\mathrm{f}} + \Delta\epsilon) \quad (5)$$

where $E_{\mathrm{Defect}}^{\mathrm{tot}}$ and $E_{\mathrm{Bulk}}^{\mathrm{tot}}$ are the total energies of the defective and pristine supercells, respectively, n_i is the number of constituent atoms exchanged upon defect formation, with chemical potentials μ_{i}, q is the charge of the defect, ε_{f} the Fermi level of the pristine cell. Moreover, $\Delta\epsilon$ is an electrostatic term aligning the core levels of the perfect and defective supercells in order to account for the Fermi level shift due to the compensating jellium background charge. Finite temperature and partial pressure formation energies were obtained by including the partial pressure dependencies and tabulated temperature dependencies on all atomic chemical potentials in Eq. 5, according to:

$$\mu_{\mathrm{i}} = \mu_i + \mu_i(T,p) + \mathrm{k_b}T\mathrm{RE}(\tfrac{p_i}{p}) \quad (6)$$

where μ_i^0 are set to the total energies of the pure phases as obtained through DFT, while $\mu_i(T, p_0)$ are the tabulated temperature dependencies of the atomic chemical potentials [31]. This approach effectively neglects contributions from vibrational changes within the crystal itself upon defect formation. However, to estimate trends in the solid state vibrational contributions to the thermodynamics of the hydration reaction (Eq. 1), we have applied a simplified Boltzmann model where all vibrational modes are assumed purely harmonic and independent, with their free energies given by:

Field Code Changed

$$G_i(T) = \frac{\mathrm{h}\nu_i}{2} + \mathrm{k_b}T\ln[1 - \exp(-\frac{\mathrm{h}\nu_i}{\mathrm{k_b}T})] \quad (7)$$

where ν_i are the vibrational frequencies. The first term thus represents the vibrational zero-point contributions to the enthalpy, while the second term represents the vibrational entropic contributions from a given lattice model.

Finally, finite temperature/pressure defect concentrations are obtained from the defect formation energies according to:

$$\frac{[\mathrm{defect}]}{[\mathrm{site}]} = \mathrm{N_{config}}\exp\left(-\frac{\Delta \mathrm{G^f_{defect}}(T,P)}{\mathrm{k_b}T}\right) \quad (8)$$

where [site] is the concentration of sites on which the defect may form (*e.g.* concentration of $O_O^\times$) and $\mathrm{N_{config}}$ is the number of configurations per site the defect may attain.

5 Results and discussion

5.1 Thermogravimetric measurements

Figure 1 displays the concentration of water in $RE_2Sn_2O_7$ (RE=La, Sm, Er) as function of inverse temperature determined from TG measurements in wet air (p_{H_2O} = 0.025 atm). The water uptake increases with decreasing temperature, reflecting the exothermic nature of the hydration reaction (Eq. 1). In the case of $La_2Sn_2O_7$ nominally doped with 0.20 mol Ca/mol oxide, the water concentration levels off at temperatures below ~450 °C. Given that thermal equilibrium is reached at the lower temperatures, this saturation reflects the limiting electroneutrality $[Ca'_{RE}] = [OH^\bullet_O]$. The saturation level (~0.042 mol H_2O/mol oxide for $La_2Sn_2O_7$) corresponds to an effective acceptor concentration of 0.084 mol Ca/mol oxide (given $[Ca'_{La}] = [OH^\bullet_O]$). This observation is in line with the segregation of $CaSnO_3$ observed in the XRD diffractograms (not shown here) indicating that the nominal acceptor concentration is beyond the solubility limit. At a given temperature (in the unsaturated

regime), the water uptake decreases in the order La→ Sm → Er, and $Sm_2Sn_2O_7$ and $Er_2Sn_2O_7$ are moreover saturated at lower temperatures than $La_2Sn_2O_7$, thus indicating an effect of the RE ion on the hydration thermodynamics.

Water uptake in nominally acceptor doped systems can be explained by a simplified defect model where water dissolves according to the reaction in Eq. 1 with the acceptor concentration, $[\mathrm{Ca}'_{\mathrm{RE}}]$, thus being charge-compensated according to:

$$\left[\mathrm{Ca}'_{\mathrm{RE}}\right] = 2[\mathrm{v}_{\mathrm{O}}^{\bullet\bullet}] + [\mathrm{OH}_{\mathrm{O}}^{\bullet}] \tag{9}$$

The hydration thermodynamics corresponding to the measured water uptake may be quantified by the mass action law;

$$K_{\mathrm{Hydr}} = \frac{\left(\frac{[\mathrm{OH}_{\mathrm{O}}^{\bullet}]}{N_{\mathrm{s,OH_O}} N_{\mathrm{c,OH_O}}}\right)^2}{\frac{[\mathrm{v}_{\mathrm{O}}^{\bullet\bullet}]}{N_{\mathrm{s,v_O}} N_{\mathrm{c,v_O}}} \cdot \frac{[\mathrm{O}_{\mathrm{O}}^{\times}]}{N_{\mathrm{s,O_O^\times}}} \cdot \frac{p_{\mathrm{H_2O}}}{p^0}} = \exp\left(\frac{\Delta_{\mathrm{hydr}} S}{\mathrm{R}}\right) \exp\left(-\frac{\Delta_{\mathrm{hydr}} H}{\mathrm{R}T}\right) \tag{10}$$

where $N_{\mathrm{s,i}}$ and $N_{\mathrm{c,i}}$ are the concentration of sites and number of configurations per site, respectively. As both oxygen vacancies and protons mainly form on the O48f (see section 4.2), of which there are 6 per formula unit, $N_{\mathrm{s,i}}$ equals 6 for both defects. Further, there is only one possible vacancy configuration per oxygen site and $N_{\mathrm{s,v_O}} = 1$. In case of protons, the most stable position is close to the O48f ions, with a 96g symmetry (according to our DFT calculations), hence $N_{\mathrm{c,OH_O}} = 2$. Finally, for small defect concentrations, $\frac{[\mathrm{O}_{\mathrm{O}}^{\times}]}{N_{\mathrm{s,O_O^\times}}}$ is taken as unity. Combination of Eq. 9 and 10 yields the proton concentration;

$$[\mathrm{OH}_{\mathrm{O}}^{\bullet}] = \frac{K_{\mathrm{Hydr}} N_{\mathrm{s,v_O}} N_{\mathrm{c,v_O}}}{4\left(N_{\mathrm{s,OH_O}} N_{\mathrm{c,OH_O}}\right)^2} \left(\frac{p_{\mathrm{H_2O}}}{p}\right) \left(-1 + \sqrt{1 + \frac{8\left(N_{\mathrm{s,OH_O}} N_{\mathrm{c,OH_O}}\right)^2 \left[\mathrm{Ca}'_{\mathrm{RE}}\right]}{K_{\mathrm{Hydr}} N_{\mathrm{s,v_O}} N_{\mathrm{c,v_O}} \left(\frac{p_{\mathrm{H_2O}}}{p}\right)}}\right) \tag{11}$$

The standard enthalpy and entropy of hydration of the $RE_2X_2O_7$ series were obtained by curve fitting of Eq. 11 to the TG profiles, with $\left[\mathrm{Ca}'_{\mathrm{RE}}\right] = 0.084$ mol/mol oxide as a first approximation The fitted curves are included in Figure1 and the extracted hydration enthalpies of Ca-doped $RE_2Sn_2O_7$ (RE=La, Sm, Er) equals $\Delta_{\mathrm{Hydr}}H$ = -103 ±5 kJ/mol, $\Delta_{\mathrm{hydr}}H$ = -76 ±8 kJ/mol and $\Delta_{\mathrm{hydr}}H$ = -44 ±10 kJ/mol, respectively.

5.2 First principles defect calculations

General defect chemistry of pyrochlores

The defect chemistry of acceptor doped pyrochlores depends on the relative formation energies of the aforementioned defects where the concentrations must follow the electroneutrality condition:

$$2[\mathrm{v_{O48f}}] + 2[\mathrm{v_{O8b}}] + [\mathrm{OH_{O48f}}] + [\mathrm{OH_{O8b}}] = \left[\mathrm{OH_{i8a}^{/}}\right] + 2\left[\mathrm{O_{i8a}^{//}}\right] + \left[\mathrm{Ca_{RE}^{/}}\right] \quad (12)$$

with defect concentrations given by Eq. 8. Figure 2 displays the equilibrium defect formation energies (with reference at the equilibrium Fermi level) at 800 K with $p_{\mathrm{H_2O}}$ = 0.025 atm and $p_{\mathrm{O_2}}$ = 1 atm for the series $Sm_2X_2O_7$ ()(X=Ti, Sn, Zr, Ce) with $\left[\mathrm{Ca_{RE}^{/}}\right]$ = 0.01 mol / mol oxide.

The most prominent change through the series is the stabilization of the two interstitial defects ($\mathrm{O_{i8a}^{//}}$ and $\mathrm{OH_{i8a}^{/}}$), and the two defects at the O8b site ($\mathrm{OH_{O8b}}$ and $\mathrm{v_{O8b}}$) with increasing size of the X-site ion (or decreasing r_{RE}/r_X). Hence, while such defects are in complete minority in $Sm_2Ti_2O_7$, their concentration will be significant in $Sm_2Ce_2O_7$, in agreement with earlier computational studies indicating that the stability of anti-Frenkel pairs increases with decreasing r_{RE}/r_X [32, 33]. Hence, while defect formation mainly occurs on the O48f site for larger r_{RE}/r_X, pyrochlores with more similar cations display a large degree of anion disorder among and occupation of the different oxygen sites in for instance the cerates is close to indistinguishable. However, the effect of order/disorder on hydration properties is outside the scope of the present study and it is presented in[25, 34].

Figure 3 displays the defect concentrations in $Sm_2Sn_2O_7$ and $Sm_2Zr_2O_7$ as function of inverse temperature with $p_{\mathrm{H_2O}}$=0.025 atm and $p_{\mathrm{O_2}}$= 1 with $\left[\mathrm{Ca_{La}^{/}}\right] = 0.01$ mol fractions. As elaborated in the preceding paragraph, the most notable difference is the stabilization of the $\mathrm{O_{i8a}^{//}}$ in the larger zirconate, which manifests itself in a dominating anti-Frenkel disorder at the highest temperatures. At lower temperatures however, these defects are predicted to be in minority with respect to the frozen-in acceptors. The dominating positive defects are in all cases $\mathrm{v_{O48f}^{\bullet\bullet}}$ and/or $\mathrm{OH_{O48f}^{\bullet}}$ which charge-compensate the acceptor according to Eq. 9. The concentration of $\mathrm{OH_{O48f}^{\bullet}}$ increases with decreasing temperature and the materials are predicted to saturate and be completely dominated by $\mathrm{OH_{O48f}^{\bullet}}$ at the lowest temperatures, in agreement with the TG measurements (see Figure 1). Finally, protons are predicted to

Field Code Changed

Field Code Changed

Field Code Changed

Field Code Changed

dominate up to slightly higher temperatures in $Sm_2Zr_2O_7$ compared to $Sm_2Sn_2O_7$ (see Figure 3).

Hydration enthalpy trends through the $RE_2X_2O_7$ series

The dominance of protons or oxygen vacancies is given by their relative formation energies, which may be quantified by the enthalpy of the hydration reaction (Eq. 1). Computationally, the hydration enthalpy is obtained through:

$$\Delta_{\mathrm{hydr}}H^{\mathrm{electronic}} = 2\Delta H^{\mathrm{f}}_{\mathrm{OH}^{\bullet}_{\mathrm{O48f}}} - \Delta H^{\mathrm{f}}_{\mathrm{v}^{\bullet\bullet}_{\mathrm{O48f}}} \quad (13)$$

Note that the enthalpies calculated according to Eq. 13 are purely of electronic nature and thus neglect zero-point vibrational contributions and contributions stemming from the temperature dependency on the chemical potential of H_2O(g). Figure 4 presents the calculated $\Delta_{\mathrm{hydr}}H^{\mathrm{electronic}}$ as function of the ionic radius of the RE ion (RE=La-Lu) through the $RE_2X_2O_7$ series (X = Ti, Sn, Zr, Ce) when constraining the structure to that of an ordered pyrochlore. Within each X-site series, the hydration enthalpy increases (less negative) with decreasing size of the RE cation, *i.e.* in the order La→Lu with a close to linear dependency. Hence, the $RE_2X_2O_7$ oxides with the larger RE ions will be dominated by protons to higher temperatures than those with the smaller RE ion, in good agreement with the TG measurements. Changing the X-site ion has less impact; the hydration enthalpy increases only slightly in the order Ti, Zr → Sn → Ce.

Vibrational contributions to the hydration thermodynamic

To estimate the solid state vibrational contributions to the hydration thermodynamics, we assume that the majority of these contributions are due to creation of 3 additional lattice modes upon formation of each $\mathrm{OH}^{\bullet}_{\mathrm{O48f}}$ defect (one O-H stretch and two O-H wag modes) and the creation of 3 lattice modes upon filling of a $\mathrm{v}^{\bullet\bullet}_{\mathrm{O48f}}$ (given by the vibrational modes of a single O48f atom), while the changes in the vibrational modes of the surrounding atoms are neglected. With the free energy of each vibrational mode given by Eq. 7 and by accounting for the zero-point energy of H_2O, the Gibbs energy of hydration is obtained through (under $p_{\mathrm{H_2O}}$ = 1 atm);

$$\Delta_{\mathrm{hydr}}G(T) = \Delta_{\mathrm{hydr}}H^{\mathrm{electronic}} + 2\left\{\sum_{i=1}^{3}\frac{\mathrm{h}\nu_{i,\mathrm{OH}^{\bullet}_{\mathrm{O48f}}}}{2} + \mathrm{k_b}T\ln[1-\exp(-\frac{\mathrm{h}\nu_{i,\mathrm{OH}^{\bullet}_{\mathrm{O48f}}}}{\mathrm{k_b}T})]\right\} +$$

$$\left\{\sum_{i=1}^{3}\frac{\mathrm{h}\nu_{i,\nu_{i,\mathrm{O}^{\times}_{\mathrm{O}}}}}{2} + \mathrm{k_b}T\ln[1-\exp(-\frac{\mathrm{h}\nu_{i,\nu_{i,\mathrm{O}^{\times}_{\mathrm{O}}}}}{\mathrm{k_b}T})]\right\} - \left\{\sum_{i=1}^{3}\frac{\mathrm{h}\nu_{i,\mathrm{H2O}}}{2} + H_{\mathrm{H2O}}(T) - S_{\mathrm{H2O}}(T)\right\} \quad (14)$$

where $\nu_{i,\mathrm{H2O}}$ are obtained from DFT calculations; 3840, 3730 and 1585 cm^{-1}. Linearization of Eq. 14 vs. T yields the standard hydration enthalpy and entropy ($\Delta_{\mathrm{hydr}}H$ and $\Delta_{\mathrm{hydr}}S$). $\Delta_{\mathrm{hydr}}H$ derived from Eq. 14 consequently contains zero-point contributions from H_2O and the additional lattice modes and a contribution due to $H_{\mathrm{H2O}}(T)$, in addition to the electronic part, $\Delta_{\mathrm{hydr}}H^{\mathrm{electronic}}$, from the preceding section. $\Delta_{\mathrm{hydr}}S$ is similarly composed of the entropy of H_2O(g) itself and the contributions due to excitation of the included lattice modes.

Table 1 lists the vibrational frequencies of the calculated modes of the $\mathrm{OH}^{\bullet}_{\mathrm{O48f}}$ defect and those of an O48f atom in selected $RE_2X_2O_7$ compositions, as well as the corresponding $\Delta_{\mathrm{hydr}}H$ and $\Delta_{\mathrm{hydr}}S$, compared with $\Delta_{\mathrm{hydr}}H^{\mathrm{electronic}}$ from the preceding section. For all compositions, the $\Delta_{\mathrm{hydr}}H^0$ is somewhat higher than $\Delta_{\mathrm{hydr}}H^{\mathrm{electronic}}$ due to inclusion of zero-point energies, but the change is comparable for all compositions due to the minor changes in the vibrational frequencies through the series. Further, the $\Delta_{\mathrm{hydr}}S$ is in the lower limit of the average value of -120±40 J/molK as usually found experimentally for similar oxides, which may reflect the simplifications of the model. Nevertheless, all entropies are less negative than -215.15 J/molK as obtained when neglecting all solid state contributions in Eq. 14, showing the significance of such contributions in the hydration reaction. There is only a minor change in the entropies through the series due to small changes in the vibrational frequencies, which again reveals only minor structural changes through the series. From Eq. 14, the low-frequency modes, *i.e.* the O48f modes and the two O-H wag modes, dominate the solid state vibrational contributions to $\Delta_{\mathrm{hydr}}S$. While the two O-H wag modes are comparable for different series of oxides, the O modes are more dependent of the bonding environment and structure. Hence, we suggest that the hydration entropy is comparable for structurally similar oxides without large symmetry changes (*e.g.* within the pyrochlore series) while it may vary more between different structural classes (*e.g.* pyrochlore vs. perovskite vs. monazite). Hence, the major change in the hydration thermodynamics through the pyrochlore series is $\Delta_{\mathrm{hydr}}H^{\mathrm{electronic}}$, which we will elaborate upon further in the following section.

Effect of bonding and electronic structure on defect stability

As formation of both $OH_{O48f}^{\bullet}$ and $v_{O48f}^{\bullet\bullet}$ represents forming and breaking various bonds, the individual contributions to the hydration enthalpy may be addressed from changes in the site projected electronic density of states (DOS) upon defect formation.

As illustrated in Figure 5 for $Sm_2Ti_2O_7$, $OH_{O48f}^{\bullet}$ formation and $v_{O48f}^{\bullet\bullet}$ consumption results in;

- Inclusion of H bonding states (Figure 5a) - 'E_{H}' in Table 2
- Stabilization of the O48f ions as represented by the downward shift in O48f states upon O-H bond formation (Figure 5a) – 'ΔE_{O48f}'
- Filling of $v_{O48f}^{\bullet\bullet}$ which is represented by the bulk O48f bonding states in Figure 5a – 'E_{O48f}'
- Shift in nearest neighbor RE and X ion states upon $OH_{O48f}^{\bullet}$ formation and $v_{O48f}^{\bullet\bullet}$ consumption (Figure 5b) –'ΔE_{RE}' and 'ΔE_{X}'

These contributions may be quantified by changes in the band energy as represented by the integrated partial DOS, E_i^{DOS}, for given ions;

$$E_i^{\mathrm{DOS}} = \sum_{\varepsilon_i=-\infty}^{\varepsilon_i=\varepsilon_{\mathrm{VBM}}} D(\varepsilon_i)\varepsilon_i \Delta\varepsilon \qquad (15)$$

where $D(\varepsilon_i)$ is the calculated DOS at energy ε_i. Table 2 summarizes the resulting band energies of the different contributions. The trend in the $\Delta_{\mathrm{hydr}}H^{\mathrm{band}}$ matches the trend of $\Delta_{\mathrm{hydr}}H^{\mathrm{electronic}}$; the enthalpies become less exothermic with decreasing RE radii, and only slightly less exothermic in the order Ti, Zr→Sn→Ce. The individual contributions indicate that these trends are due both to changes in the stability of $OH_{O48f}^{\bullet}$ and $v_{O48f}^{\bullet\bullet}$. In the series Sm→Er→Lu, both the energy gain of forming two $OH_{O48f}^{\bullet}$ and that of filling the $v_{O48f}^{\bullet\bullet}$ decreases (*i.e.* less stable protons and more stable oxygen vacancies) with decreasing RE size. The change is mostly due to a decreasing contribution from ΔE_{O48f} (OH stability) and E_{O48f} (decreasing stability of O48f ions). However, upon changing the X-site ion, changes in the different contributions are to some extent counteracting: The energy gain of forming two $OH_{O48f}^{\bullet}$ decreases (less stable protons) in the order Sn→Zr→Ce→Ti, whereas that from filling a $v_{O48f}^{\bullet\bullet}$ increases (less stable vacancies) in the order Sn→Ce→Zr→Ti. Overall, this results in a less pronounced overall effect on the hydration enthalpy. The fact that ΔE_{O48f} and E_{O48f} change in a concise manner through the RE-ion series indicates that these contributions and changes in the hydration enthalpy through the series may be related to changes in the

bonding nature (degree of covalency) and stability of the O48f ions (or stability of the oxide). Effects of changing the X-site ion seem less conclusive and such factors change and affect the defect stability and hydration thermodynamics in a more complicated manner.

Bonding nature

Table 3 lists the Bader charges of the RE, X, O8b and O48f ions for selected $RE_2X_2O_7$ compositions as emerging from the Bader partitioning of the bulk systems. Within the $RE_2Ti_2O_7$ series, the charge of the RE cation increases (more positive) while that of the two oxide ions decreases somewhat (more negative) in the order Sm→Lu, thus indicating increased ionic character through the series. There is a similar effect of changing the X-site ion; the X-site ions become more positive and the O48f ions become more negative in the order Ti → Sn → Zr, while there is only a minor change on the Sm and O8b ions, indicating increasing ionic character of the X-O48f bond. Further, the change in the O48f ion polarization upon X-ion substitution is approximately twice that of the change from La to Lu.

In the literature, one of the hypotheses has been that hydration of oxygen vacancies correlates with the basicity of the oxides. The basicity, and $\Delta_{\mathrm{hydr}}H$ in principle should correlate with the Bader charges of the O48f ions. However, we do not observe any such simple correlation in this work (Figure 4 and Table 3). Interesting, the change in the Bader charge of the O48f is most pronounced upon changing the X-site ion, *i.e.* opposite to the change in $\Delta_{\mathrm{hydr}}H$. Further, from the band energies in the preceding section (see Table 2), it is clear that the $\Delta_{\mathrm{hydr}}H$ trend from La→Lu is due both to destabilization of protons and stabilization of vacancies, which thus mainly may be attributed to the decreasing oxide stability through the RE series. Similarly, upon changing the X-site ion, the defects are affected by changes in the oxide ion stability, but the change is to some extent counteracted by the more pronounced change in the degree of ionicity and O48f polarization, and the $\Delta_{\mathrm{hydr}}H$ thus change in a more complex manner with upon changing the X-site ion.

5.3 General hydration trends

As elaborated in the preceding section, the hydration enthalpy of $RE_2X_2O_7$ pyrochlores for a given X-ion correlates with the size of the RE-ion is attributed to destabilization of the oxide and increasing degree of ionicity for smaller RE ions. Figure 6 displays the obtained hydration enthalpies versus the calculated oxide formation enthalpies (Figure 6a) and the

r_{RE}/r_X ratio (Figure 6b). There is no clear trend in neither the formation enthalpy nor in the r_{RE}/r_X ratio that applies to all series. However, within a given X-ion series, the hydration enthalpy clearly correlates with both parameters, as both reflect the stability and bonding nature of the oxides.

The hydration enthalpy of rare-earth pyrochlores displays the opposite dependence on the RE ion compared to rare-earth sesquioxides (RE_2O_3)[2] and rare-earth ortho-niobates ($RENbO_4$)[18], although their formation enthalpies follow the same trend through the RE series. This may thus indicate larger changes in the O-ion polarization upon reduction of the RE ion size than in the pyrochlores. Nevertheless, also in these systems, changing the X-site ion has a smaller effect on the hydration properties than the RE-ion (*i.e.* $LaPO_4$, $LaAsO_4$, $LaVO_4$)[7, 8] which as for the pyrochlores can be due to counteracting effects from changes in O-ion polarization and stability of the oxides.

For ABO_3 perovskite oxides, the hydration enthalpy has been correlated with the difference in electronegativity of the A and B cations[1, 20] and related to the basicity of the oxide ions. However as elaborated in this study, we believe this trend is due to changes in the oxide stability and degree of ionicity, which also is reflected by that both the hydration and formation enthalpy of perovskite structured oxides to some extent correlate with the Goldschmidt's tolerance factor[20]. A detailed study of the stabilization of protons and oxygen vacancies with bonding nature and stability of the oxides through different classes of oxides will be pursued to elaborate on more general hydration trends.

Field Code Changed
Field Code Changed
Field Code Changed
Field Code Changed
Field Code Changed
Field Code Changed
Field Code Changed

6. Summary

Comparative DFT calculations and TG measurements have been employed to elucidate the trends in the defect chemistry and hydration properties through the pyrochlore structured $RE_2X_2O_7$ (RE = La-Lu and X = Ce, Zr, Sn, Ti) series of compounds. The DFT calculations revealed that the dominating positive defects in all studied systems are $v_{O48f}^{\bullet\bullet}$ and/or $OH_{O48f}^{\bullet}$ which charge-compensate frozen-in acceptors. In systems with smaller r_{RE}/r_X, the interstitial defects $O_{i8a}^{//}$ and $OH_{i8a}^{/}$, and defects at the second oxygen site, OH_{O8b} and v_{O8b}, are stabilized, and such oxides therefore display a large degree of anion disorder. Consequently, systems with large X-site ions, such as cerates, are predicted to behave as disordered systems with defect formation occurring among the different oxygen sites, whereas systems with smaller X-site ion behave as ordered pyrochlores with defect formation occurring on the O48f sites.

Total energy and phonon calculations within the DFT approximation reveal that trends in the hydration thermodynamics through the pyrochlore series to a large extent is dominated by electronic (binding) contributions. Hydration entropies obtained from phonon calculations and a simplified Boltzmann model are comparable for all included series due to only small changes in the vibrational characteristics of oxygen ions and protons. The hydration enthalpies obtained with DFT calculations become more exothermic with increasing size of RE ion, while the effect of changing the X-site element is smaller. These computational findings are in good agreement with TG measurements on Ca doped $RE_2Sn_2O_7$ (RE = La, Sm, Er), which show increasing water uptake (at a given temperature) and more exothermic hydration enthalpies with increasing RE size

The relative contribution from formation of protons and filling of oxygen vacancies to the hydration enthalpy was quantified by integration of the calculated partial DOS. The increasing hydration enthalpy with decreasing RE-ion size is attributed to destabilization of protons and stabilization of oxygen vacancies, *i.e.* additive contributions, through the series. This stabilization is attributed to both increasing stability of the oxide and increasing degree of ionicity in the same order. The smaller effect of changing the X-site element is similarly attributed to counteracting contributions from stabilization of both protons and oxygen vacancies. Hence, within each X-ion series, the hydration enthalpies correlate with the size of the RE ion, or the r_{RE}/r_X ratio, while no general trends applying to all series was found.

Table 1: Calculated vibrational frequencies of modes corresponding to the $OH^{\bullet}_{O48f}$ defect and an O48f atom, $\Delta_{hydr}H^{electronic}$ as reported in Figure 4, and $\Delta_{hydr}H^{0}$and $\Delta_{hydr}S^{0}$ as obtained through linearization of Eq. 14.

	$OH^{\bullet}_{O48f}$ / cm^{-1}			O48f / cm^{-1}			$\Delta_{hydr}H^{electronic}$	$\Delta_{hydr}H$	$\Delta_{hydr}S$
	ν_1	ν_2	ν_3	ν_1	ν_2	ν_3	kJ/mol	kJ/mol	J/molK
$Sm_2Zr_2O_7$	3531	826	719	590	320	312	-77	-68	-165
$Sm_2Ti_2O_7$	3410	829	780	533	344	306	-77	-68	-166
$Sm_2Sn_2O_7$	3431	998	771	579	370	283	-70	-60	-168
$Er_2Sn_2O_7$	3471	980	790	623	372	297	-23	-12	-170
$La_2Sn_2O_7$	3471	980	790	623	372	297	-91	-82	-167

Table 2: Band energy of various contributions to the hydration enthalpy from integration of the partial DOS; inclusion of H bonding states (E_H), downward shift of O48f states upon OH formation (ΔE_{O48f}), shifts in RE (ΔE_{RE}) and X (ΔE_X) states due to $OH^{\bullet}_{O48f}$ formation and filling of $v^{\bullet\bullet}_{O48f}$, the energy gain of filling an $v^{\bullet\bullet}_{O48f}$, (energy of an O48f ion, ΔE_{O48f}) and the sums of the contributions from the two defects and the corresponding 'band hydration energy'.

	Formation of $OH^{\bullet}_{O48f}$ (×2) /eV					**Filling of $v^{\bullet\bullet}_{O48f}$ / eV**				$\Delta_{hydr}H^{band}$
	E_H	ΔE_{O48f}	ΔE_{RE}	ΔE_X	Sum	E_{O48f}	ΔE_{RE}	ΔE_X	Sum	/ eV
Lu$_2$Ti$_2$O$_7$	-5.4	-7.0	-0.1	+1.4	-11.1	-18.6	-1.4	+0.2	-19.9	-42.0
Er$_2$Ti$_2$O$_7$	-5.4	-7.1	-0.1	-0.6	-13.0	-18.6	-0.6	-1.3	-20.5	-46.5
Sm$_2$**Ti**$_2$O$_7$	-5.4	-7.6	-0.5	+0.1	-13.3	-20.8	-1.8	-0.8	-23.4	-50.0
Sm$_2$**Zr**$_2$O$_7$	-6.2	-9.1	-0.4	-0.4	-16.1	-17.8	-1.8	+2.4	-17.2	-49.4
Sm$_2$**Sn**$_2$O$_7$	-5.0	-10.9	+1.4	-5.2	-19.6	-25.1	+1.9	+13.8	-9.4	-48.6
Sm$_2$**Ce**$_2$O$_7$	-5.4	-8.9	+0.2	-0.5	-14.7	-15.3	-2.3	+4.8	-12.8	-42.2

Table 3: *Bader charges of selected pristine $RE_2X_2O_7$ compositions.*

	RE	**X**	**O8b**	**O48f**
$Sm_2Zr_2O_7$	2.18	2.57	-1.39	-1.35
$Sm_2Sn_2O_7$	2.18	2.46	-1.38	-1.31
$Sm_2Ti_2O_7$	2.16	2.34	-1.37	-1.27
Gd_2**Ti_2O_7**	2.23	2.34	-1.44	-1.28
Er_2**Ti_2O_7**	2.28	2.35	-1.48	-1.30

Figure 1

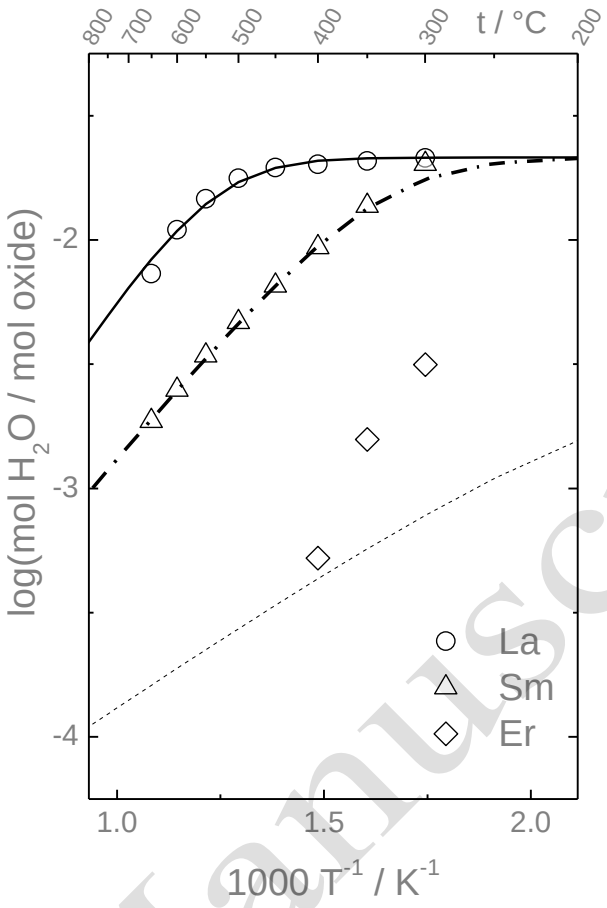

Figure 1: Water uptake in Ca doped $RE_2Sn_2O_7$ (RE=La, Sm, Er) as function of inverse temperature in wet air. The symbols represent the water uptake as measured by means of TG, while the lines correspond to curve fitting of the data according to Eq.10.

Figure 2

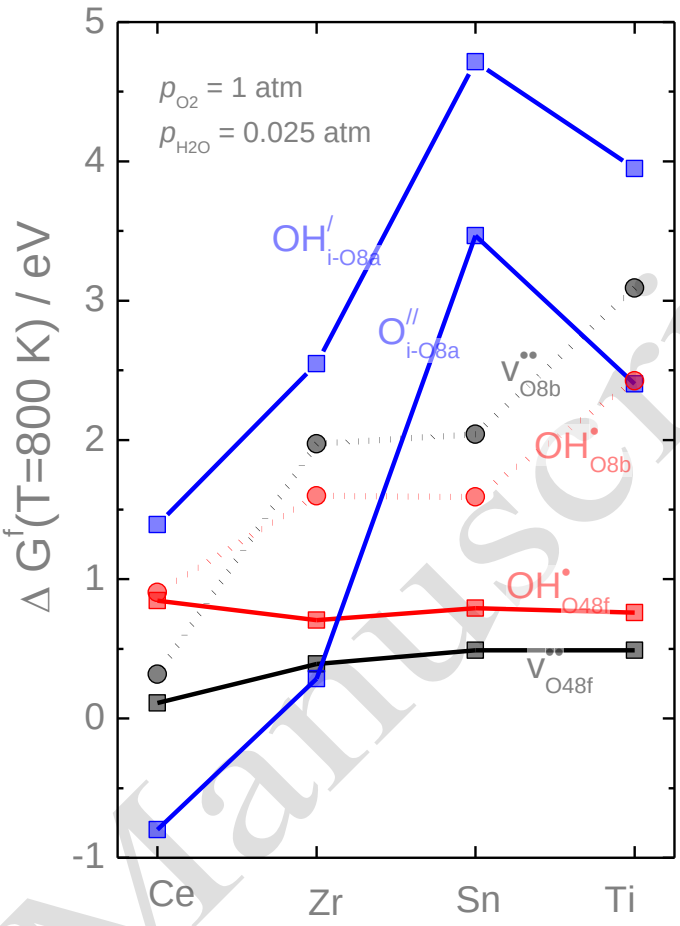

Figure 2: Equilibrium defect formation energies in the series $Sm_2X_2O_7$ (X=Ti, Sn, Zr, Ce) at 800 K, p_{H_2O}=0.025 and p_{O_2}=1 atm as obtained when solving the electroneutrality with $[Ca'_{RE}] = 0.01$ mol fractions

Figure 3

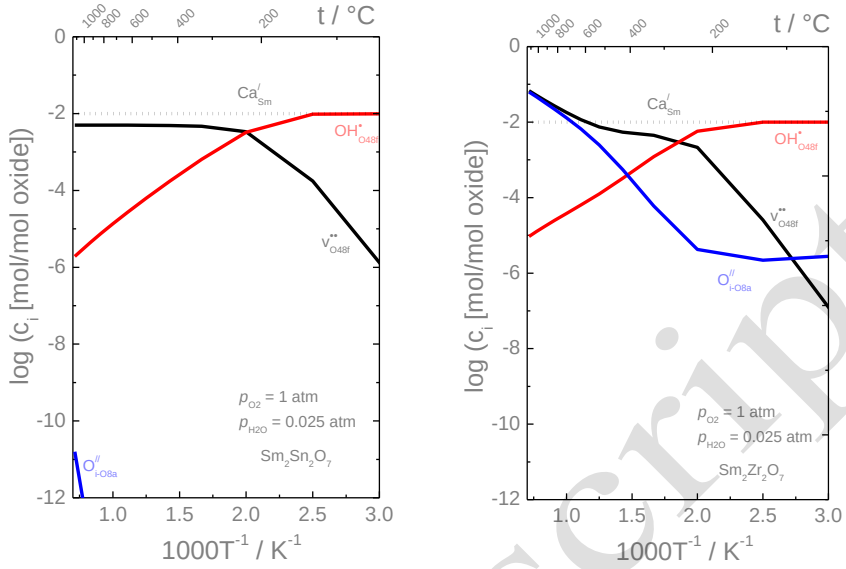

(a) (b)

Figure 3: Thermal equilibrium defect concentrations under wet, oxidizing conditions (p_{H_2O}=0.025 and p_{O_2}=1) in $Sm_2Sn_2O_7$ and $Sm_2Zr_2O_7$ with $[Ca'_{RE}] = 0.01$ mol fractions.

Figure 4

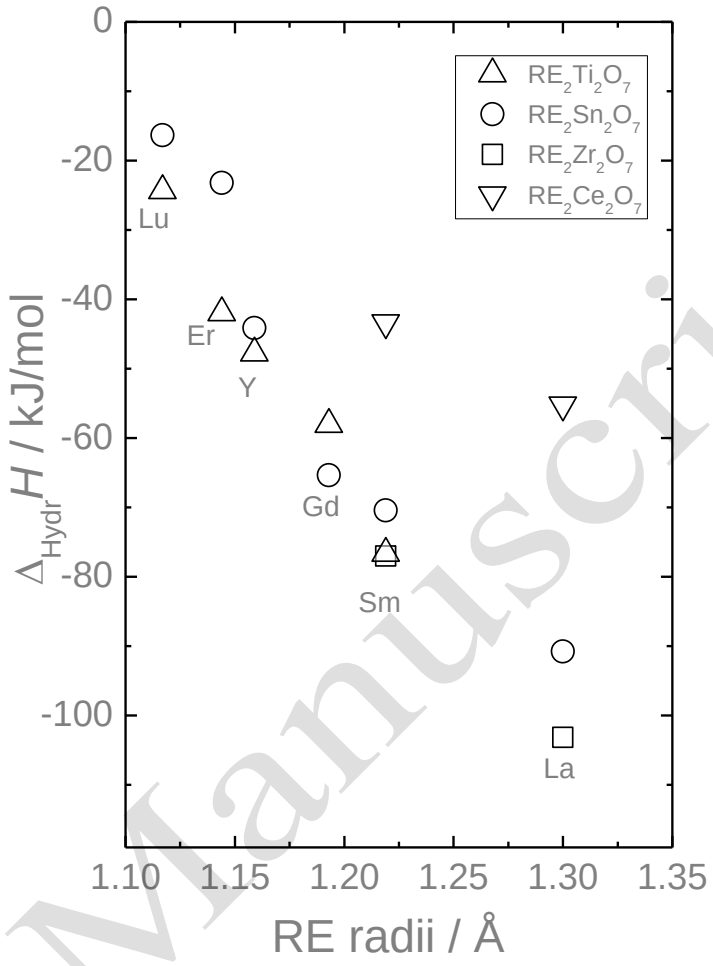

Figure 4: Calculated hydration enthalpies (excluding zero point vibrational contributions) for selected pyrochlore structured $RE_2X_2O_7$ compositions (X = Ti, Sn, Zr, Ce).

Figure 5

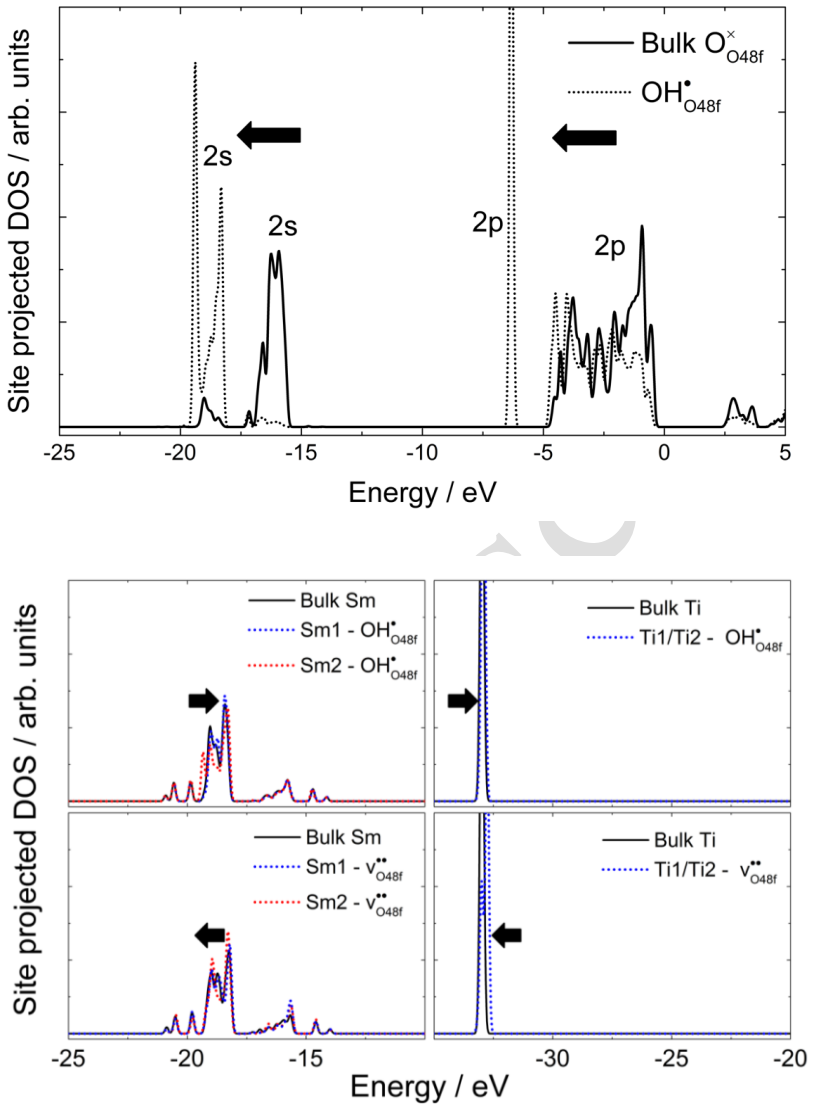

Figure 5: Site projected DOS in $Sm_2Ti_2O_7$ for (a) $O^{\times}_{O}$ and $OH^{\bullet}_{O}$ and (b) cations in bulk and on sites next to $OH^{\bullet}_{O}$ and $v^{\bullet\bullet}_{O}$, respectively. The valence band top is set to 0 eV.

Figure 6

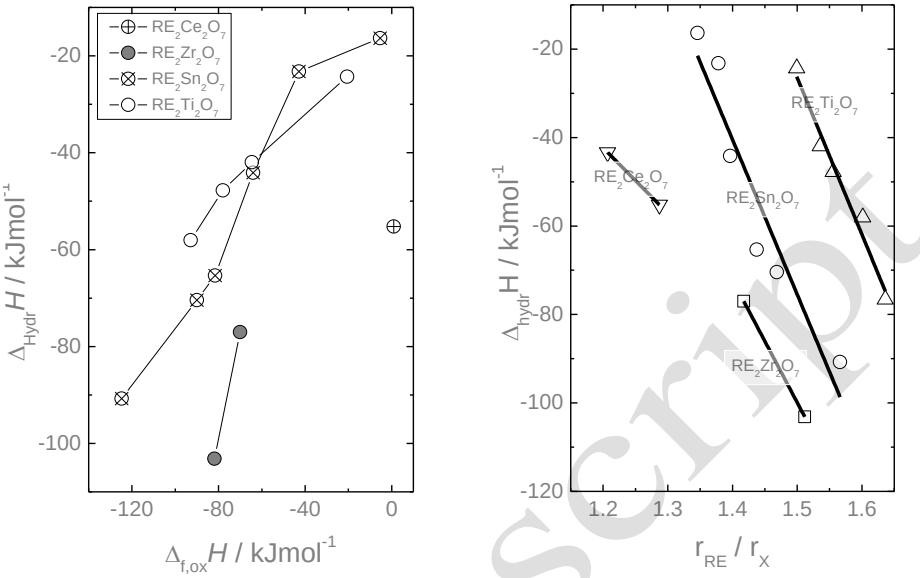

(a) (b)

Figure 6: Hydration enthalpies versus the formation enthalpy (from DFT calculations) and the r_{RE}/r_X ratio of the ternary $RE_2X_2O_7$ (X=Ti, Sn, Zr, Ce) oxides.

References

1. T. Norby, M. Wideroe, R. Glockner and Y. Larring, *Dalton Transactions*, 2004, 3012-3018.
2. Y. Larring and T. Norby, *Solid State Ionics*, 1995, **77**, 147-151.
3. K. D. Kreuer, S. Adams, W. Münch, A. Fuchs, U. Klock and J. Maier, *Solid State Ionics*, 2001, **145**, 295-306.
4. K. D. Kreuer, *Ann. Rev. Mater. Res.*, 2003, **33**, 333-359.
5. H. G. Bohn and T. Schober, *Journal of the American Ceramic Society*, 2000, **83**, 768-772.
6. T. Norby and N. Christiansen, *Solid State Ionics*, 1995, **77**, 240-243.
7. M. Huse, T. Norby and R. Haugsrud, *Journal of The Electrochemical Society*, 2011, **158**, B857-B865.
8. T. S. Bjørheim, T. Norby and R. Haugsrud, *Journal of Materials Chemistry*, 2012, **22**.
9. R. Haugsrud and T. Norby, *Nat Mater*, 2006, **5**, 193-196.
10. R. Haugsrud and T. Norby, *Solid State Ionics*, 2006, **177**, 1129-1135.
11. T. Omata and S. Otsuka-Yao-Matsuo, *J. Electrochem. Soc.*, 2001, **148**, E252-E261.
12. K. E. J. Eurenius, E. Ahlberg, I. Ahmed, S. G. Eriksson and C. S. Knee, *Solid State Ionics*, **In Press, Corrected Proof**.
13. K. E. J. Eurenius, E. Ahlberg and C. S. Knee, *Dalton Transactions*, 2011, **40**, 3946-3954.
14. M. E. Björketun, C. S. Knee, B. J. Nyman and G. Wahnström, *Solid State Ionics*, 2008, **178**, 1642-1647.
15. T. Shimura, M. Komori and H. Iwahara, *Solid State Ionics*, 1996, **86-8**, 685-689.
16. T. Omata, K. Ikeda, R. Tokashiki and S. Otsuka-Yao-Matsuo, *Solid State Ionics*, 2004, **167**, 389-397.
17. T. Omata, K. Okuda, S. Tsugimoto and S. Otsuka-Matsuo-Yao, *Solid State Ionics*, 1997, **104**, 249-258.
18. R. Haugsrud and T. Norby, *Nature Materials*, 2006, **5**, 193-196.
19. T. Tauer, R. O'Hayre and J. W. Medlin, *Solid State Ionics*, 2011, **204–205**, 27-34.
20. T. S. Bjørheim, A. Kuwabara, I. Ahmed, R. Haugsrud, S. Stølen and T. Norby, *Solid State Ionics*, 2010, **181**, 130-137.
21. T. Norby and Y. Larring, *Current Opinion in Solid State and Materials Science*, 1997, **2**, 593-599.
22. H. Fjeld, R. Haugsrud, A. E. Gunnæs and T. Norby, *Solid State Ionics*, 2008, **179**, 1849-1853.
23. J. A. Díaz-Guillén, M. R. Díaz-Guillén, K. P. Padmasree, A. F. Fuentes, J. Santamaría and C. León, *Solid State Ionics*, 2008, **179**, 2160-2164.
24. P. K. Moon, in *Department of Materials Science and Engineering*, Massachusetts Institute of Technology, Cambridge, MA, 1988.
25. S. R. Vasileios Besikiotis, Molly Hjorth Jensen, Truls Norby, Reidar Haugsrud, 2012.
26. G. Kresse and J. Furthmüller, *Physical Review B*, 1996, **54**, 11169.
27. G. Kresse and D. Joubert, *Physical Review B*, 1999, **59**, 1758.
28. J. P. Perdew, K. Burke and M. Ernzerhof, *Physical Review Letters*, 1996, **77**, 3865.
29. P. E. Blöchl, *Physical Review B*, 1994, **50**, 17953.
30. G. Henkelman, A. Arnaldsson and H. Jónsson, *Computational Materials Science*, 2006, **36**, 354-360.
31. M. W. Chase Jr., *NIST-JANAF Thermochemical Tables*, The American Institute of Physics for The National Institute of Standards and Technology, New York, 1998.
32. P. J. Wilde and C. R. A. Catlow, *Solid State Ionics*, 1998, **112**, 173-183.
33. Licia Minervini, Robin W. Grimes and Kurt E. Sickafus, *Journal of the American Ceramic Society*, 2000, **83**, 1873-1878.
34. V. B. L. Kalland, R. Haugsrud, T. Norby, in *Materials Research Society, Spring Meeting*, Materials Research Society, San Francisco CA, USA, 2012.